

Simplifying FFT-based methods for mechanics with automatic differentiation

Mohit Pundir^a, David S. Kammer^{a,*}

^a*Institute for Building Materials, ETH Zurich, Switzerland*

Abstract

Fast-Fourier Transform (FFT) methods have been widely used in solid mechanics to address complex homogenization problems. However, current FFT-based methods face challenges that limit their applicability to intricate material models or complex mechanical problems. These challenges include the manual implementation of constitutive laws and the use of computationally expensive and complex algorithms to couple microscale mechanisms to macroscale material behavior. Here, we incorporate automatic differentiation (AD) within the FFT framework to mitigate these challenges. We demonstrate that AD-enhanced FFT-based methods can derive stress and tangent stiffness directly from energy density functionals, facilitating the extension of FFT-based methods to more intricate material models. Additionally, AD simplifies the calculation of homogenized tangent stiffness for microstructures with complex architectures and constitutive properties. This enhancement renders current FFT-based methods more modular, enabling them to tackle homogenization in complex multiscale systems, especially those involving multiphysics processes. Our work will simplify the numerical implementation of FFT-based methods for complex solid mechanics problems.

Keywords: Spectral method, Automatic differentiation, Multiscale, Homogenization

1. Introduction

A crucial aspect of computational mechanics is understanding how microscale mechanisms impact macroscale material behavior. Features such as the distribution of heterogeneities, the formation of structures at the micro level, and physical processes occurring on the microscale can significantly influence the properties homogenized at a larger scale. The Fast-Fourier Transform (FFT) methods [1, 2, 3] are particularly well-suited for tackling such homogenization problems due to their computational efficiency [4, 5], ease of implementation [6], and low memory footprint. Nonetheless, certain aspects of FFT frameworks limit their quick adaptation to various applications and extension to intricate mechanical systems.

A significant challenge with FFT-based methods is that they still rely on manually implemented stress-strain relationships, which are computed “by hand” either analytically or through numerical differentiation [4]. This makes the implementation of complex constitutive relations (*e.g.*, hyperelastic materials and elastoplastic materials) intricate

*Corresponding author

Email addresses: mpundir@ethz.ch (Mohit Pundir), dkammer@ethz.ch (David S. Kammer)

and error-prone within the FFT framework, especially for cases involving multi-physical processes [7]. Hence, one of their major strength (*i.e.* ease of implementation) is lost for more complex problems. Another prominent limitation lies in determining the homogenized tangent stiffness in multiscale simulations [8, 9, 10, 11]. Current FFT-based multiscale frameworks require auxiliary solution schemes [12] to couple microscale mechanisms to the macroscale through a constitutive tangent stiffness, which can be computationally expensive and inaccurate for complex material models and large computational domains.

Other numerical methods have similar challenges, which have been overcome by adopting a differentiable framework, which automates the process of computing derivatives [13]. This allows the formulation of the governing equation in a high-level manner (usually as an expression of the functional energy), and the complex Jacobian and the Hessian are then strictly derived through automatic differentiation (AD) up to machine precision [7, 14]. Among prominent examples of such differentiable frameworks within the field of solid mechanics is FEniCSx [15] for Finite Element Methods. Concurrently, with the rise of automatic differentiation (AD) libraries such as pyTorch [16] and JAX [17], the differentiable framework has become quite appealing, which is evident by the shift in porting existing frameworks such as molecular dynamics, discrete element method, and finite element method [18, 19, 20, 21, 22] to a differentiation-based framework. Similarly, AD presents great potential for FFT-based methods [23] but has yet to be developed in a general and ease-of-use manner to overcome the main challenges of FFT-based methods.

In this (short) paper, we enhance the FFT framework by incorporating automatic differentiation. We investigate the capabilities of an AD-enhanced FFT framework and examine how automatic differentiation mitigates some of the aforementioned issues. Thereby making FFT-based frameworks more modular and easy to implement for complex mechanical problems.

2. Differentiable FFT-framework for solid mechanics

For the purpose of this work, we incorporate automatic differentiation within the Fourier-Galerkin approach [2] for FFT-based solvers. To this end, we explore the specific arithmetic operations made more straightforward by automatic differentiation and present the relevant pseudo-code/algorithm.

Consider a Representative Volume Element (RVE) Ω subjected to an overall strain $\bar{\epsilon}$. The governing equation for static mechanical equilibrium in this RVE is thus given by $\nabla \cdot \boldsymbol{\sigma} = \mathbf{0}$, where $\boldsymbol{\sigma}$ is a function/operator that maps the overall deformation to the appropriate local stress field. Under small-strain conditions, the overall deformation $\bar{\epsilon}$ represents small-strain $\boldsymbol{\epsilon}$, and $\boldsymbol{\sigma}$ represents a function that maps local $\boldsymbol{\epsilon}$, to the Cauchy stress tensor $\boldsymbol{\tau}$. Conversely, for finite deformations, $\bar{\epsilon}$ represents the deformation gradient $\bar{\mathbf{F}}$ and $\boldsymbol{\sigma}$ represents a function that maps the local deformation gradients \mathbf{F} to the first Piola-Kirchhoff stress tensor \mathbf{P} . Since this paper addresses both conditions, we will use the stress operator $\boldsymbol{\sigma}$ as a generic term for stresses in the description of the method throughout this section. We note that, consequently, the derivations and procedures remain consistent for both assumptions.

In this study, we adopt the Fourier-Galerkin spectral method [2, 3], and do so for several reasons. Primarily, the variational structure of this approach retains the convexity of the energy density [3, 4], which ensures that a unique solution to a given problem exists. Secondly, to guarantee that the solution produces a compatible strain state, the

method employs a projection operator \mathbb{G} , which converts an arbitrary strain state to a compatible state (periodic and curl-free). This operator is independent of the material model and remains consistent for both small-strain and finite deformation scenarios [6]. Finally, unlike other methods [1], the Fourier-Galerkin method does not rely on a reference medium stiffness tensor, which can impact the convergence in nonlinear problems [6]. We will show that these characteristics of the Fourier-Galerkin approach make integrating automatic differentiation within the FFT-based framework straightforward.

Applying the Fourier-Galerkin method, we reformulate the static equilibrium equation as

$$\mathcal{F}^{-1}\{\widehat{\mathbb{G}}(\boldsymbol{\xi}) : \widehat{\boldsymbol{\sigma}}(\boldsymbol{\xi})\} = \mathbf{0} , \quad (1)$$

where $\boldsymbol{\xi}$ is the wavevector, $\widehat{\star}(\boldsymbol{\xi})$ is the Fourier transform of quantity \star , and $\mathcal{F}^{-1}\{\star\}$ is the inverse Fourier transform. For details on the derivation of the above equation and the exact form of the projection operator \mathbb{G} , please refer to [2, 3, 6, 24]. The above equation is solved using a Newton-Krylov solver, where the Newton-Raphson loop is employed to handle nonlinearities, and a Krylov-subspace solver, such as Conjugate Gradient, is employed to enforce the compatibility conditions (for details, see Appendix A).

Here, we will show how automatic differentiation can be applied in an FFT-based framework. We will describe three use cases of AD, namely the stress computation in elastic and hyperelastic materials, the computation of consistent tangent operator for nonlinear problems, and the computation of homogenized stiffness operator for multi-scale simulations. For all cases, we include both the arithmetic operations as well as the counterpart pseudo-code to highlight the general applicability and ease of use of AD in FFT-based methods. To this end, we employ the open-source JAX library [17] for automatic differentiation and demonstrate that only a few lines of code are needed to implement a general solution.

First, we consider the stress computation of elastic and hyperelastic materials, for which the stress function $\boldsymbol{\sigma}$ is the first derivative of the strain energy density, as given by

$$\boldsymbol{\sigma}(\boldsymbol{x}) = \frac{\partial \psi(\boldsymbol{e})}{\partial \boldsymbol{e}} . \quad (2)$$

The application of automatic differentiation on Eq. 2 using the JAX library [17] is straightforward:

```
def strain_energy(strain):
    # compute the energy based on the input `strain`
    return energy

# create a function to compute stresses using the
# derivative of energy w.r.t `strain` (Eq 2)
compute_stresses = jax.jacfwd(strain_energy)

# using the above created function to compute stresses
sigma = compute_stresses(strain)
```

Here, we define a function that receives microscale strain as input and outputs the corresponding energy density. A function to calculate stresses can then be derived using the forward differentiation technique [13, 17]. We note that the input strain to the strain-energy function may be either a small strain ($\boldsymbol{\varepsilon}$) or a deformation gradient (\boldsymbol{F}) based

on the defined energy density. In Sec. 3.1, we will present examples for various material models under small-strain and finite deformation settings.

Next, we integrate automatic differentiation to ease the numerical implementation of the nonlinear form of Equation (1). In standard practice, Equation (1) is linearized, and the Newton-Raphson method is used to find the equilibrium. The linearization process involves computing the incremental stresses and the consistent tangent operator at each step of the Newton-Raphson scheme, which is expressed as follows,

$$\delta\boldsymbol{\sigma} = - \underbrace{\frac{\partial\boldsymbol{\sigma}(\mathbf{e})}{\partial\mathbf{e}}}_{\mathbb{K}} \delta\mathbf{e} . \quad (3)$$

Consequently, the local tangent stiffness \mathbb{K} is needed at the previous strain for the computation of the incremental stresses. With automatic differentiation, the incremental stress can be computed as follows

```
# create a function to compute stresses
compute_stresses = jax.jacfwd(strain_energy)

# computing the incremental stresses as given in Eq 3
dsigma = jax.jvp(compute_stresses, (prev_strain,), (dstrain,))[1]
```

Here, we utilize a JAX functionality to represent the local tangent stiffness as a push-forward function (or a linear operator) that maps incremental strains $\delta\mathbf{e}$ lying in the tangent space of \mathbf{e} to the incremental stresses $\delta\boldsymbol{\sigma}$ lying in the tangent space of the stress domain. This facilitates the direct computation of incremental stress as a Jacobian-vector product [25, 26]. Furthermore, representing \mathbb{K} as a push-forward map instead of explicitly storing it in a matrix form is expected to reduce the memory footprint of FFT-based methods significantly.

Lastly, we exploit the automatic differentiation technique to compute the homogenized stiffness tensor, which is the most significant aspect of computational homogenization [27, 28, 29] or the essential requirement for performing multiscale simulations [12, 30]. The effective stiffness tensor is the partial derivative of macroscale stresses with respect to macroscale strains, which reads

$$\bar{\mathbb{C}} = \frac{\partial\bar{\boldsymbol{\sigma}}}{\partial\bar{\mathbf{e}}}, \quad \text{where} \quad \bar{\boldsymbol{\sigma}} = \frac{\int_{\Omega} \boldsymbol{\sigma}(\mathbf{e}(\mathbf{x}))d\Omega}{\int_{\Omega} d\Omega}, \quad (4)$$

where $\bar{\boldsymbol{\sigma}}$ is the volume average of local stresses within the RVE. In the FFT-based framework, two methods are used to determine the effective properties from the local stress and strain distribution: (a) the perturbation approach [12, 31] and (b) the algorithmic consistent approach [32]. In the perturbation approach, each component of the effective tensor is computed by numerical differentiation (finite difference) between the perturbed state and the reference state. In the algorithmic consistent approach, the consistent tangent operator is computed by solving the Lippmann-Schwinger equation [32]. Both approaches necessitate an auxiliary solution method alongside the primary one to determine effective properties. For instance, the perturbation method requires computing finite differences for every tensor component, leading to three computations in a 2D case and six in a 3D case. Similarly, resolving the Lippmann-Schwinger equation requires an iterative solver.

Consequently, both approaches can be computationally intensive, especially for large computational domains or for nonlinear constitutive laws. In contrast to these approaches, AD significantly simplifies the procedure by employing a single operation for the computation of the homogenized tangent stiffness, as shown below:

```

# function to solve RVE using FFT approach for a given macroscale strain
def solve_microscale(macro_strain):
    # solve RVE (Eq 1) using Newton-Krylov solver as given in Appendix A
    # and get the microscale strain
    local_strain = netwon_krylov_solver(macro_strain)

    # compute the microscale stresses from microscale strain
    local_sigma = compute_stresses(local_strain)

    # compute the macroscale stresses from microscale stress
    macro_sigma = mean(local_sigma)
    return macro_sigma, (macro_sigma)

# create a function to compute homogenized tangent and stresses
compute_macro_tangent_stiffness = jax.jacfwd(
    solve_microscale, argnums=0, has_aux=True
)

# calling tangent function to get macroscale stresses and tangents
macro_tangent, macro_stress = compute_macro_tangent_stiffness(macro_strain)

```

Here, we directly differentiate a function that takes macro-strain as input and outputs macro-stress (after solving Equation (2)) to compute the homogenized stiffness tensor. This function encompasses numerous complex operations or function calls, such as forward-FFT transform, inverse FFT transform, and a Newton-Krylov solver, to accurately determine the local strain and stress distribution in an RVE (for details, refer [6, 24]). The ability of AD to decompose complicated arithmetic operations into primitive ones allows for exact differentiation. Moreover, it facilitates the simultaneous computation of stresses and tangent stiffness, thus eliminating the need for any secondary solution method.

3. Applications

Incorporating automatic differentiation in an FFT-based framework can, as described in Section 2, greatly simplify the method, which is essential for many mechanical problems. Here, we employ the AD-enhanced Fourier-Galerkin method on problems of varying complexity to demonstrate its capabilities. Specifically, we examine mechanical problems with intricate material models, bodies undergoing large-strain deformation, and multiscale simulations. We evaluate the computational performance and accuracy of the AD-enhanced FFT-based method and show how automatic differentiation simplifies the approach. We provide the Python code for all the examples at [33]. All simulations were performed as a serial job on a Linux system using a 4-core AMD EPYC™ 9654 CPU with 16 GB RAM and a clock speed of 2.4Hz.

3.1. Automatic derivation of stress and tangent operator

We present two examples to demonstrate the applicability of AD for the computation of stress and tangent operators for material laws with fundamentally different characteristics, *i.e.* hyperelastic and elastoplastic materials.

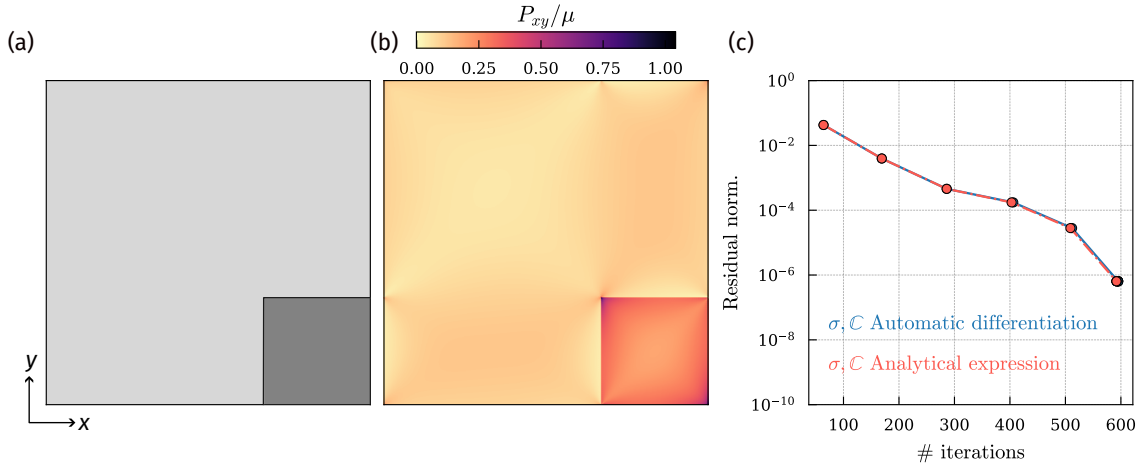


Figure 1: Automatic computation of stress and tangent operator for a St. Venant-Kirchhoff material. (a) Schematic illustration of the microstructure of the considered RVE. (b) Local distribution of the first Piola-Kirchhoff stresses within the RVE. (c) Variation of the residual norm and the cumulative CG iterations for each NR iteration (shown as circles).

3.1.1. Example on hyperelastic material

With this example, we aim to show the reliance of FFT-based frameworks on explicit formulations for stress and tangent operators can be minimized [4]. We consider *hyperelastic* materials, where the stress-strain relationship is directly derived from the strain energy density functional. We consider the St. Venant-Kirchhoff material for which the energy density functional is given as

$$\psi = \frac{\lambda}{2} \text{tr}(\mathbf{E})^2 + \mu \text{tr}(\mathbf{E} : \mathbf{E}) , \quad (5)$$

where $\mathbf{E} = \mathbf{F} \cdot \mathbf{F}^T - \mathbf{I}$ is the Green-Lagrange strain, \mathbf{F} is the deformation gradient, λ and μ are Lamé's parameters. As described in Section 2, we apply AD to derive the stress function (the Jacobian of the energy density) and the tangent function (the Hessian of the energy density).

Foremost, we compare the AD implementation for St. Venant-Kirchhoff material with the implementation where the stress and tangent functions are computed from the analytical expression. Similar to [6], we consider a square RVE of dimension ℓ (see Figure 1a) with a square stiff inclusion (of dimension $\ell/3$) at one of its corners. The RVE is subjected to a macroscopic shear loading in terms of $\bar{\mathbf{F}}$ which in Voigt notation is given as $[1, 1, 1 + 0.1\ell]$. We discretize the RVE into 299^2 grid points. An odd number of grid points is chosen to maintain the compatibility of the deformation gradient [3]. We solve the problem in one increment using a Newton-Krylov solver with a conjugate gradient (CG) solver for solving the linearized form of Equation (1). The tolerance for the outer Newton-Raphson (NR) loop is 10^{-5} , and the tolerance for the inner loop of the CG solver is 10^{-8} . We compute the local distribution of the first-Piola Kirchhoff stresses within the RVE (see Figure 1b) and the residual norm ($\delta \mathbf{F} / \|\bar{\mathbf{F}}\|$) for every NR iteration (see Figure 1c). The AD implementation gives identical results to the analytical expression, as the residual norm and the iteration counts (cumulative CG iterations for every NR iteration) to reach convergence are the same. The computational times for the simulations with AD

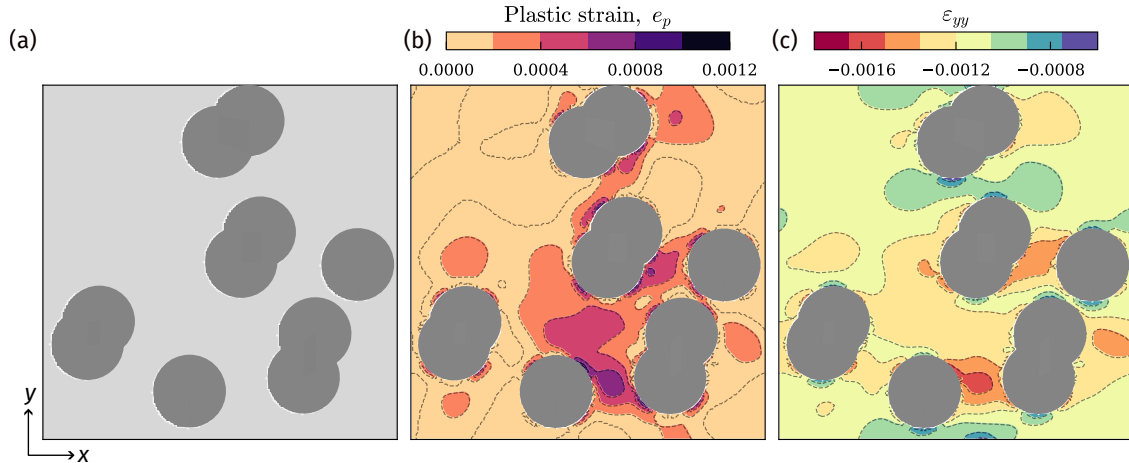


Figure 2: Automatic computation of tangent operator for J2 plasticity. (a) The microstructure of the considered RVE. The stiff circular inclusions have a higher yielding strength than the matrix. (b) Distribution of cumulative plastic strain ϵ_p and (c) local distribution of strain within the RVE. The color map is the result of AD-enhanced FFT simulations, and the dashed contour lines represent the results of the analytical implementation of the elastoplastic material.

implementation and with analytical implementation are approximately the same, around 19.5 seconds. Since we express the tangent operator as a function rather than storing it as a matrix, the memory footprint of the AD-enhanced version of our implementation is roughly 1/2 of that of the analytical expression.

This example demonstrates that stress and the tangent operator can be easily derived from an energy functional for a material. This approach eliminates the need for FFT-based methods to rely on analytical expressions or numerical differentiation, thereby reducing computational cost (*i.e.*, memory usage) and simplifying the numerical implementation of sophisticated hyperelastic materials.

3.1.2. Example on elastoplastic material

Automatic differentiation is applicable to material laws in which the stresses and the tangent stiffness cannot be explicitly derived from the energy density. For instance, elastoplastic materials involve stress and tangent computations that depend on yielding criteria, plastic flow rule, and a return-mapping algorithm [34]. For demonstration purposes, we consider a heterogeneous RVE with stiff circular inclusions embedded in a soft matrix (see Figure 2a). We adopt an isotropic linear hardening model in a small-strain setting with each phase exhibiting distinct hardening exponents and yield stresses. The RVE is subjected to a macroscopic biaxial loading, in terms of $\bar{\epsilon}$ which in Voigt notation is given as $[10^{-2}\ell, 10^{-2}\ell, 0]$. The RVE is discretized into 199^2 grid points. The tangent stiffness operator in elastoplastic materials depends on the elastic strain, the plastic strain, the type of yield surface, and the normals to this yield surface [35, 34]. We chose J2 plasticity for which the consistent constitutive tangent is equal to the elastic tangent when the trial state is elastic and otherwise given as,

$$\mathbb{K} = \frac{\partial \boldsymbol{\sigma}^t}{\partial \mathbf{e}^t} = \mathbb{C}_e - \frac{6G^2 \Delta\gamma}{\text{tr}\boldsymbol{\sigma}_{\text{eq}}} I_d + 4G^2 \left(\frac{\Delta\gamma}{\text{tr}\boldsymbol{\sigma}_{\text{eq}}} - \frac{1}{3G + nH(\epsilon_p^{(t)} + \Delta\gamma)} \right)^{n-1} \text{tr}N \otimes \text{tr}N .$$

	$\bar{\mathbb{C}}_{xxxx}$	$\bar{\mathbb{C}}_{yyyy}$	$\bar{\mathbb{C}}_{xyxy}$
Analytical	4.037	4.037	1.011
Numerical	4.035	4.035	1.010

Table 1: Components of the effective elastic tensor \mathbb{C} as computed numerically by automatic differentiation using FFT solvers compared against Eshelby’s solution for a stiff inclusion embedded in a soft infinite matrix.

Automatic differentiation calculates the tangent stiffness on the fly by differentiating the stresses with respect to the strains. Unlike the previous case of hyper-elastic material, where the local stiffness tangent operator is computed as a double derivative of an energy density function, here we first implement a Python function to compute the correct stress state. This is done using a return mapping algorithm [35, 34]. Then, this function is automatically differentiated with respect to the input. For details on the numerical implementation of an elastoplastic material for an AD-enhanced FFT-based method, see the pseudo-code in [Appendix B](#).

We observe that the local distribution of the plastic strain and the elastic strain (see [Figure 2b](#) and [Figure 2c](#)) for the AD-computed local tangent stiffness operator \mathbb{K} matches the strains computed with the analytical expression of \mathbb{K} (shown with dashed contour lines in [Figure 2](#)). We note that the computation time for the AD implementation and the analytical implementation was approximately the same, around 0.25 seconds. We believe that as the analytical expression for calculating the tangent stiffness grows more intricate, the analytical implementation begins to slow down due to the surge in arithmetic operations. In such scenarios, AD, with its straightforward process for implementing tangent stiffness and comparable computational performance, becomes more advantageous.

Through this example, we show that a local stiffness operator can also be achieved for the cases where the stresses are not a direct derivative of the energy functional. This increases the applicability of AD to various other material models where the calculation of stresses involves complex computational functions or operations.

3.2. Computational homogenization

We apply the AD-enhanced FFT-based framework to perform computational homogenization of an RVE. As noted earlier, current approaches, such as numerical differentiation or the algorithmic consistent approach, require an auxiliary computationally intensive method to compute the homogenized stiffness tensor of an RVE. Here, we present two examples to illustrate the efficacy and efficiency of AD in computing effective properties.

First, we consider the Eshelby problem as a basic example to compare the numerical result against the analytical solution. To this end, we model a periodic micro-structure with a stiff circular inclusion embedded in a soft matrix. We compare the numerically computed effective elastic tensor $\bar{\mathbb{C}}$ with Eshelby’s solution. We consider a very low volume fraction of the inclusion to match the infinite medium assumption of Eshelby, as commonly done [32]. The material parameters chosen for the matrix are $\lambda_m = 2$ GPa and $\mu = 1$ GPa, and for the stiff inclusion are $\lambda_i = 10$ GPa and $\mu_i = 5$ GPa. We observe that the results from the AD implementation are close to the analytical results (see [Table 1](#)). While an in-depth comparison of computational cost with the above-mentioned approaches is beyond the scope of this paper, we note that for a computational grid of 199^2 , the total computation time was around 4 sec.

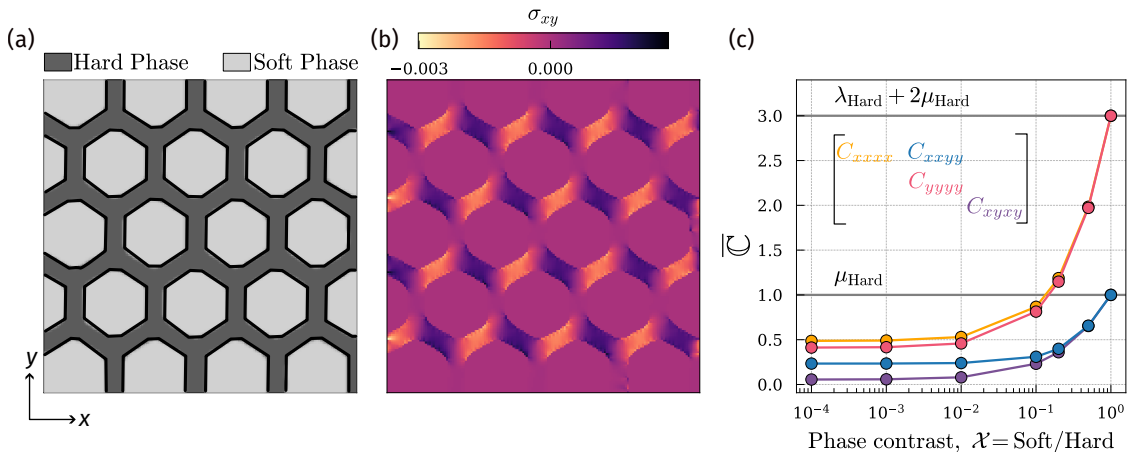


Figure 3: Computational homogenization of an architected lattice material. (a) The architected RVE with a hard phase arranged in a hexagonal pattern within a soft phase. (b) Local distribution of shear stresses within the RVE for a phase contrast of $\mathcal{X} = 0.5$ and a macroscopic strain $\bar{\epsilon} = [-10^{-3}\ell, -10^{-3}\ell, 0]$. (c) Components of the macroscale constitutive tangent stiffness as a function of phase contrast \mathcal{X} . The dark grey horizontal lines show the stiffness component for the homogeneous case *i.e.* $\mathcal{X} = 1$.

Next, we apply the AD-enhanced computational homogenization method to an RVE (of dimension ℓ) with intricate microstructure. We chose architected materials as our example. Architected materials are composed of two or more distinct phase materials arranged in a specific pattern that results in exceptional mechanical properties [36, 37, 38]. We examine a two-phase linear elastic architected material as illustrated in Figure 3a, comprising a soft phase and a hard phase, where the hard phase is arranged in a hexagonal pattern. We vary the phase contrast $\mathcal{X} = \text{soft}/\text{hard}$ from 1 to 10^{-4} where a value of 1 represents a homogeneous material and value $\ll 1$ approximates a lattice metamaterial [39]. We apply a macroscopic compressive strain $\bar{\epsilon}$ in x and y -directions under a small-strain setting. The macroscopic strain tensor in Voigt notation is given as $[-10^{-3}\ell, -10^{-3}\ell, 0]$. For the case where $\mathcal{X} = 1$, *i.e.* a homogeneous material, the computed macro stiffness values match the analytical solution (see Figure 3c). With increasing phase contrast, however, the macroscopic stiffness reduces, as expected, and converges to values that are indicative of lattice metamaterials. This demonstrates that the AD-enhanced approach is able to handle substantial contrast in phase properties.

3.3. Application to multiscale problem

For our final application, we showcase how the ease of computation of homogenized stiffness tensor allows seamless integration of the AD-enhanced FFT-based framework with an additional solver. To this end, we explore a multiscale framework where the macroscale problem is tackled using the Finite Element Method (FEM), while the microscale problem employs the FFT-based approach. This example demonstrates the flexibility of the AD-enhanced FFT-based method by integrating it with a FEM solver.

The macroscale problem involves a beam with dimensions $L \times H$, where the left end is fixed in both the x and y directions. A displacement of $10^{-2}L$ is applied to the right edge along the y -axis (see Figure 4a). At the microscale, we use the same composite RVE as in Section 3.2 but with the St. Venant-Kirchhoff material model to capture the geometric nonlinearity (see Equation (5)). A phase contrast of 0.01 is chosen between the soft

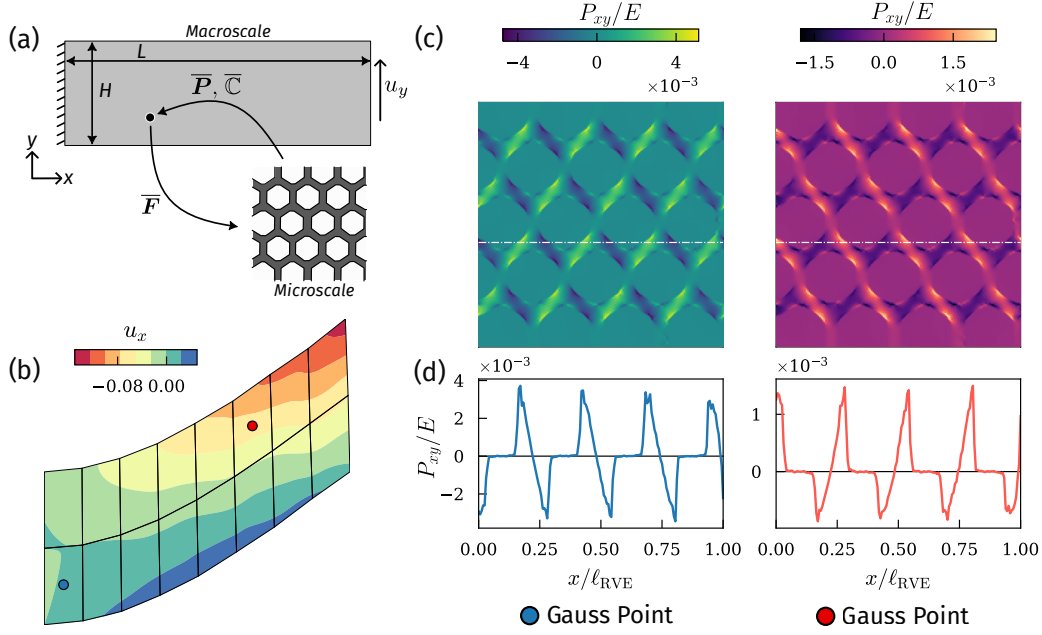


Figure 4: Multiscale simulation of a hyperelastic lattice material. (a) Schematic illustration of the beam at the macroscale and the hexagonal lattice structure at the microscale. (b) The deformed state of the beam for an applied displacement of $10^{-2}L$. The color corresponds to the macroscale displacement along the x -axis. The finite element discretization is shown by black lines and two Gauss points are highlighted by colored (red and blue) points. (c) The local shear stress distribution within the RVEs associated with the 2 Gauss points highlighted in (b). (d) Normalized shear stress profile along line highlighted by white dashes in (c).

and hard phases to represent voids, thus modeling a hexagonal-lattice metamaterial. We solve the macroscale problem in reference configuration with \mathbf{P} and \mathbf{F} as the stress-strain measures. The weak form at the macroscale thus reads,

$$\int_V \underbrace{\bar{\mathbf{C}}(\mathbf{F}) : \bar{\mathbf{F}}}_{\bar{\mathbf{P}}} : \nabla \bar{\mathbf{u}} \cdot dV = 0, \quad \text{where} \quad \bar{\mathbf{C}} = \frac{\partial \bar{\mathbf{P}}}{\partial \bar{\mathbf{F}}}, \quad (6)$$

where the homogenized tangent operator $\bar{\mathbf{C}}$ is computed from microscale. We discretize the beam into 16 quadrilateral finite elements (16 Gauss points) as shown in Figure 4b, where each Gauss point is linked to the RVE with 169^2 voxels. The deformation gradient $\bar{\mathbf{F}}$ at each Gauss point within the macroscale domain is transferred as input to the corresponding RVE associated with that specific Gauss point. Similar to the previous example, we determine the homogenized tangent operator $\bar{\mathbf{C}}$ through AD and pass it together with the average first-Piola Kirchhoff stress $\bar{\mathbf{P}}$ to the FEM solver (see Figure 4a). We note that due to a non-symmetric deformation gradient, one needs to use a full deformation gradient (4 components) [31]. This means that $\bar{\mathbf{C}}$ is a 4×4 matrix. We perform the simulation in one displacement increment under static conditions and use FEniCSx to manage the FEM component [15, 22].

At the microscale, we apply the Newton-Krylov solver (with an outer tolerance of 10^{-5} and an inner tolerance of 10^{-6}) to accurately capture the nonlinearity within the

lattices. At the macroscale, a separate Newton-Raphson solver (with a tolerance of 10^{-8}) is used to ensure proper convergence. We observe that the chosen contrast of 0.01 between the two phases sufficiently replicates the voids, which is demonstrated by the stresses in the soft phases dropping to 0, as shown by the stress profile across the cross-section in Figure 4c. We report that this simulation takes approx. 20 minutes in total (for roughly 1 million degrees of freedom in total). A large part of the computational time is spent in the CG-solver because of the high contrast in the phase properties. This is a known issue for the Fourier-Galerkin approach [40], which can be improved using pre-conditioned solvers [5]. A traditional FE-FFT framework [12], such as finite-difference-based computation of homogenized stiffness tensor, would require 4 operations per Gauss point, one for each component of non-symmetric deformation gradient, to compute $\bar{\mathbb{C}}$. Conversely, the AD-enhanced multiscale framework is notably advantageous in this scenario, as it demands only one operation per Gauss point for the same.

4. Discussion & Outlook

The integration of automatic differentiation (AD) with Fast Fourier transform (FFT) techniques can considerably simplify the numerical implementation of complex solid mechanics problems. A key advantage is the ease of deriving stress and tangent operators, thereby minimizing human error and enhancing precision. This work combines automatic differentiation with the Fourier-Galerkin method, whose variational structure facilitates straightforward integration of AD. Here, we investigated the potential of AD in FFT-based methods for mechanics, demonstrating how the automatic derivation of stress and tangent operators enables modular FFT approaches. This strengthens the use of FFT-based methods in more advanced models, particularly in multiscale scenarios where computing homogenized tangent stiffness has traditionally been a significant challenge. While we have emphasized potential applications in Section 3, several other research areas could also greatly benefit from combining AD with FFT-based methods.

A notable application in which we expect AD-based FFT-based methods to be beneficial is computational inelasticity. As shown in Section 3.1, AD greatly simplifies the extraction of the local tangent stiffness for inelastic models and is computationally equivalent to analytical expressions. Therefore, one can leverage AD for complex plasticity models such as multi-yield surface J2 plasticity [41], Simo-plasticity [34] or crystal plasticity [42, 43] for which extracting the tangent stiffness is intricate and often relies on numerical differentiation [31]. AD can also streamline the return-mapping algorithm by boosting the robustness of trial-state projections to the yield surface [35, 34]. Furthermore, multiphysical problems (or coupled problems) offer another promising avenue for the application of AD-enhanced FFT techniques [44, 45, 24]. For example, AD can support the creation of coupled or staggered operators, leading to more precise and efficient solutions for such problems. As discussed in [7], linearizing a thermo-mechanical problem requires four-tangent stiffness matrices; using AD, one can greatly simplify this number to 1 or 2. Additionally, expressing them as operators can significantly reduce the memory footprint. We demonstrated that employing AD-derived operators for the St. Venant-Kirchhoff material model, which has a straightforward analytical form (with only a few mathematical operations) for tangent stiffness, can halve memory usage.

Tackling inverse problems such as topology optimization or PDE-constrained problems can also be simplified with the integration of AD into FFT-based methods. For example,

a critical operation in such problems is the calculation of the adjoint for sensitivity analysis [21, 46]. This can be computed as a vector-Jacobian operator, a functionality provided by most auto-differentiation libraries [17]. Furthermore, by broadening AD-FFT techniques to encompass second-order homogenization and strain gradient models, one can boost the precision and predictive power of multiscale simulations, thereby expanding the limits of computational mechanics and materials science. This adaptability highlights the potential of AD in enhancing FFT-based methods for numerous mechanical applications.

5. Conclusion

In this paper, we investigated the use of automatic differentiation (AD) within the FFT-based framework for solid mechanics. We have shown that AD allows the computation of stresses and tangent operators directly from the energy density functional, which makes FFT-based methods more accessible for complex hyperelastic materials. Furthermore, we have demonstrated that AD allows differentiation of intricate tensor operations, FFT transforms, and Newton-Krylov solvers, which enable the computation of tangent operators for materials where local stiffness is not derivable from strain density, *e.g.*, elastoplastic materials. The incorporation of AD into the FFT-based framework decreases the reliance on explicit expressions of stresses and tangent operators while preserving accuracy and computational efficiency. We further employed the AD-enhanced FFT-based method to simplify the computation of homogenized stiffness tensors, a notable computational bottleneck in multiscale problems. Our findings indicate that applying AD within an FFT-based method is highly beneficial and greatly simplifies the implementation of complex solid mechanics problems, as is also evident by the simple code that we provide at [33]. We believe this research will encourage further studies using automatic differentiation within the FFT-based frameworks and will help in advancing the field of computational solid mechanics.

6. CRediT authorship contribution statement

Mohit Pundir: Conceptualization, Methodology, Formal analysis, Investigation, Software, Writing - Original Draft, Visualization; **David S. Kammer:** Writing - Review & Editing, Resources, Supervision, Funding acquisition

7. Acknowledgements

DSK and MP acknowledge support from the Swiss National Science Foundation under the SNSF starting grant (TMSGI2_211655). We thank Jan Zeman and Antoine Sanner for fruitful discussions and Alessandra Lingua for providing the scans of the lattice structure. We also thank Luca Michel for his feedback on the manuscript.

8. Code Availability

The code [33] for the simulation is written in Python and is an extension of the code provided in [24].

Appendix A. Netwon-Krylov solver

Algorithm 1 Netwon-Krylov Solver

- 1: For a given macroscopic strain $\bar{\mathbf{e}}$

 - 2: $\mathbf{r}(\mathbf{x}) = -\nabla\sigma(\bar{\mathbf{e}})$, $\mathbf{e}(\mathbf{x})^i = \bar{\mathbf{e}}$ $\triangleright \sigma(\boldsymbol{\varepsilon}) = \mathbb{C} : \boldsymbol{\varepsilon}$
 - 3: **while** true **do**
 - 4: solve : $\mathcal{F}^{-1}\{\widehat{\mathbb{G}}(\boldsymbol{\xi}) : \widehat{\boldsymbol{\sigma}}(\delta\mathbf{e})(\boldsymbol{\xi})\} = \mathcal{F}^{-1}\{\widehat{\mathbb{G}}(\boldsymbol{\xi}) : \widehat{\boldsymbol{\sigma}}(\mathbf{r})(\boldsymbol{\xi})\}$ \triangleright Linear iterative solver
 - 5: update : $\mathbf{e}(\mathbf{x})^{i+1} = \mathbf{e}(\mathbf{x})^i + \mathcal{F}^{-1}\{\widehat{\delta\mathbf{e}}(\boldsymbol{\xi})\}$
 - 6: **if** $\delta\mathbf{e}(\mathbf{x})/\|\bar{\mathbf{e}}\| < \text{tol}$ **then** break
 - 7: **else**
 - 8: $\mathbf{r}(\mathbf{x}) = -\nabla\sigma(\mathbf{e}(\mathbf{x})^{i+1})$
-

Appendix B. Computation of incremental stresses for an elastoplastic material

```
# explicit implementation of a Python function to compute stresses
def compute_stresses(strain):
    # Compute the trial state stresses
    # evaluate yield surface, set to zero if elastic (or stress-free)
    # plastic multiplier, based on hardening law
    # apply return-map algorithm to project stresses to a feasible state
    return sigma
# computing the incremental stresses for an elasto-plastic material
dsigma = jax.jvp(compute_stresses, (prev_strain,), (dstrain,))[1]
```

References

- [1] J. C. Michel, H. Moulinec, and P. Suquet, “A computational scheme for linear and non-linear composites with arbitrary phase contrast,” *International Journal for Numerical Methods in Engineering*, vol. 52, no. 1-2, pp. 139–160, 2001. eprint: <https://onlinelibrary.wiley.com/doi/pdf/10.1002/nme.275>.
- [2] J. Vondřejc, J. Zeman, and I. Marek, “An FFT-based Galerkin method for homogenization of periodic media,” *Computers & Mathematics with Applications*, vol. 68, pp. 156–173, Aug. 2014.
- [3] J. Zeman, T. W. J. de Geus, J. Vondřejc, R. H. J. Peerlings, and M. G. D. Geers, “A finite element perspective on nonlinear FFT-based micromechanical simulations,” *International Journal for Numerical Methods in Engineering*, vol. 111, no. 10, pp. 903–926, 2017. eprint: <https://onlinelibrary.wiley.com/doi/pdf/10.1002/nme.5481>.
- [4] M. Schneider, “A review of nonlinear FFT-based computational homogenization methods,” *Acta Mechanica*, vol. 232, pp. 2051–2100, June 2021.
- [5] M. Ladecký, R. Leute, and J. Zeman, *Optimal FFT-accelerated Finite Element Solver for Homogenization*. Mar. 2022.
- [6] T. W. J. de Geus, J. Vondřejc, J. Zeman, R. H. J. Peerlings, and M. G. D. Geers, “Finite strain FFT-based non-linear solvers made simple,” *Computer Methods in Applied Mechanics and Engineering*, vol. 318, pp. 412–430, May 2017.
- [7] S. Rothe and S. Hartmann, “Automatic differentiation for stress and consistent tangent computation,” *Archive of Applied Mechanics*, vol. 85, pp. 1103–1125, Aug. 2015.
- [8] M. Rambausek, F. S. Göküzüm, L. T. K. Nguyen, and M.-A. Keip, “A two-scale FE-FFT approach to nonlinear magneto-elasticity,” *International Journal for Numerical Methods in Engineering*, vol. 117, no. 11, pp. 1117–1142, 2019.
- [9] C. Gierden, J. Kochmann, J. Waimann, T. Kinner-Becker, J. Sölter, B. Svendsen, and S. Reese, “Efficient two-scale FE-FFT-based mechanical process simulation of elasto-viscoplastic polycrystals at finite strains,” *Computer Methods in Applied Mechanics and Engineering*, vol. 374, p. 113566, Feb. 2021.
- [10] J. Kochmann, L. Ehle, S. Wulfinghoff, J. Mayer, B. Svendsen, and S. Reese, “Efficient Multiscale FE-FFT-Based Modeling and Simulation of Macroscopic Deformation Processes with Non-linear Heterogeneous Microstructures,” in *Multiscale Modeling of Heterogeneous Structures* (J. Sorić, P. Wriggers, and O. Allix, eds.), pp. 129–146, Cham: Springer International Publishing, 2018.
- [11] S. Felder, J. Kochmann, S. Wulfinghoff, and S. Reese, “Multiscale FE-FFT-based thermo-mechanically coupled modeling of viscoplastic polycrystalline materials,”
- [12] C. Gierden, J. Kochmann, J. Waimann, B. Svendsen, and S. Reese, “A Review of FE-FFT-Based Two-Scale Methods for Computational Modeling of Microstructure Evolution and Macroscopic Material Behavior,” *Archives of Computational Methods in Engineering*, vol. 29, pp. 4115–4135, Oct. 2022.

- [13] C. C. Margossian, “A Review of automatic differentiation and its efficient implementation,” *WIREs Data Mining and Knowledge Discovery*, vol. 9, p. e1305, July 2019. arXiv:1811.05031 [cs, stat].
- [14] A. Vigliotti and F. Auricchio, “Automatic differentiation for solid mechanics,” *Archives of Computational Methods in Engineering*, vol. 28, pp. 875–895, May 2021. arXiv:2001.07366 [cs, math].
- [15] I. A. Baratta, J. P. Dean, J. S. Dokken, M. Habera, J. S. Hale, C. N. Richardson, M. E. Rognes, M. W. Scroggs, N. Sime, and G. N. Wells, “DOLFINx: the next generation FEniCS problem solving environment,” 2023. Published: preprint.
- [16] J. Ansel, E. Yang, H. He, N. Gimelshein, A. Jain, M. Voznesensky, B. Bao, P. Bell, D. Berard, E. Burovski, G. Chauhan, A. Chourdia, W. Constable, A. Desmaison, Z. DeVito, E. Ellison, W. Feng, J. Gong, M. Gschwind, B. Hirsh, S. Huang, K. Kalambarakar, L. Kirsch, M. Lazos, M. Lezcano, Y. Liang, J. Liang, Y. Lu, C. Luk, B. Maher, Y. Pan, C. Puhersch, M. Reso, M. Saroufim, M. Y. Siraichi, H. Suk, M. Suo, P. Tillet, E. Wang, X. Wang, W. Wen, S. Zhang, X. Zhao, K. Zhou, R. Zou, A. Mathews, G. Chanan, P. Wu, and S. Chintala, “PyTorch 2: Faster Machine Learning Through Dynamic Python Bytecode Transformation and Graph Compilation,” Apr. 2024. Publication Title: 29th ACM International Conference on Architectural Support for Programming Languages and Operating Systems, Volume 2 (ASPLOS '24) original-date: 2016-08-13T05:26:41Z.
- [17] J. Bradbury, R. Frostig, P. Hawkins, M. J. Johnson, C. Leary, D. Maclaurin, G. Necula, A. Paszke, J. VanderPlas, S. Wanderman-Milne, and Q. Zhang, “JAX: composable transformations of Python+NumPy programs,” 2018.
- [18] S. S. Schoenholz and E. D. Cubuk, “JAX M.D. A Framework for Differentiable Physics,” in *Advances in Neural Information Processing Systems*, vol. 33, Curran Associates, Inc., 2020.
- [19] M. Carrer, H. M. Cezar, S. L. Bore, M. Ledum, and M. Cascella, “Learning Force Field Parameters from Differentiable Particle-Field Molecular Dynamics,” *Journal of Chemical Information and Modeling*, July 2024. Publisher: American Chemical Society.
- [20] A. P. Toshev, H. Ramachandran, J. A. Erbesdobler, G. Galletti, J. Brandstetter, and N. A. Adams, “JAX-SPH: A Differentiable Smoothed Particle Hydrodynamics Framework,” Mar. 2024. arXiv:2403.04750 [physics].
- [21] T. Xue, S. Liao, Z. Gan, C. Park, X. Xie, W. K. Liu, and J. Cao, “JAX-FEM: A differentiable GPU-accelerated 3D finite element solver for automatic inverse design and mechanistic data science,” *Computer Physics Communications*, vol. 291, p. 108802, Oct. 2023.
- [22] J. Bleyer, “Numerical tours of Computational Mechanics with FEniCSx,” Jan. 2024.

- [23] J. Blühdorn, N. R. Gauger, and M. Kabel, “AutoMat: automatic differentiation for generalized standard materials on GPUs,” *Computational Mechanics*, vol. 69, pp. 589–613, Feb. 2022.
- [24] M. Pundir, D. S. Kammer, and U. Angst, “An FFT-based framework for predicting corrosion-driven damage in fractal porous media,” *Journal of the Mechanics and Physics of Solids*, vol. 179, p. 105388, Oct. 2023.
- [25] M. W. Hirsch, S. Smale, and R. L. Devaney, *Differential Equations, Dynamical Systems, and an Introduction to Chaos*. Elsevier, 3 ed., 2013.
- [26] R. Balestrierio and R. Baraniuk, “Fast Jacobian-Vector Product for Deep Networks,” Mar. 2021. arXiv:2104.00219 [cs].
- [27] J. D. Eshelby and R. E. Peierls, “The determination of the elastic field of an ellipsoidal inclusion, and related problems,” *Proceedings of the Royal Society of London. Series A. Mathematical and Physical Sciences*, vol. 241, pp. 376–396, Jan. 1997. Publisher: Royal Society.
- [28] L. Dormieux, D. Kondo, and F.-J. Ulm, *Microporomechanics*. John Wiley & Sons, Ltd, 1 ed., 2006.
- [29] X. Blanc and C. Le Bris, *Homogenization Theory for Multiscale Problems: An introduction*, vol. 21 of *MS&A*. Cham: Springer Nature Switzerland, 2023.
- [30] M. G. D. Geers, V. G. Kouznetsova, and W. A. M. Brekelmans, “Multi-scale computational homogenization: Trends and challenges,” *Journal of Computational and Applied Mathematics*, vol. 234, pp. 2175–2182, Aug. 2010.
- [31] F. Meier, C. Schwarz, and E. Werner, “Determination of the tangent stiffness tensor in materials modeling in case of large deformations by calculation of a directed strain perturbation,” *Computer Methods in Applied Mechanics and Engineering*, vol. 300, pp. 628–642, Mar. 2016.
- [32] F. S. Göküzüm and M.-A. Keip, “An algorithmically consistent macroscopic tangent operator for FFT-based computational homogenization,” *International Journal for Numerical Methods in Engineering*, vol. 113, no. 4, pp. 581–600, 2018.
- [33] M. Pundir and D. S. Kammer, “Supplementary Code - Simplifying FFT-based methods for mechanics with automatic differentiation (<https://gitlab.ethz.ch/cmbm-public/papers-supp-info/2024/simplifying-fft-based-methods-for-mechanics-with-automatic-differentiation>),” 2024.
- [34] J. C. Simo and T. J. R. Hughes, *Computational Inelasticity*, vol. 7. New York: Springer-Verlag, 1998.
- [35] T. Belytschko, W. K. Liu, B. Moran, and K. I. Elkhodary, *Nonlinear Finite Elements for Continua and Structures*. Wiley, 2 ed., 2014.

- [36] M. Balan P, J. Mertens A, and M. V. A. R. Bahubalendruni, “Auxetic mechanical metamaterials and their futuristic developments: A state-of-art review,” *Materials Today Communications*, vol. 34, p. 105285, Mar. 2023.
- [37] K. Karapiperis and D. M. Kochmann, “Prediction and control of fracture paths in disordered architected materials using graph neural networks,” *Communications Engineering*, vol. 2, pp. 1–9, June 2023. Publisher: Nature Publishing Group.
- [38] T. Magrini, C. Fox, A. Wihardja, A. Kolli, and C. Daraio, “Control of Mechanical and Fracture Properties in Two-Phase Materials Reinforced by Continuous, Irregular Networks,” *Advanced Materials*, vol. 36, no. 6, p. 2305198, 2024.
- [39] A. J. D. Shaikeea, H. Cui, M. O’Masta, X. R. Zheng, and V. S. Deshpande, “The toughness of mechanical metamaterials,” *Nature Materials*, vol. 21, pp. 297–304, Mar. 2022. Publisher: Nature Publishing Group.
- [40] J. Zeman, J. Vondřejc, J. Novák, and I. Marek, “Accelerating a FFT-based solver for numerical homogenization of periodic media by conjugate gradients,” *Journal of Computational Physics*, vol. 229, pp. 8065–8071, Oct. 2010. arXiv:1004.1122 [cond-mat, physics:physics].
- [41] Q. Gu, J. P. Conte, Z. Yang, and A. Elgamal, “Consistent tangent moduli for multi-yield-surface J2 plasticity model,” *Computational Mechanics*, vol. 48, pp. 97–120, July 2011.
- [42] S. Lucarini, F. P. E. Dunne, and E. Martínez-Pañeda, “An FFT-based crystal plasticity phase-field model for micromechanical fatigue cracking based on the stored energy density,” *International Journal of Fatigue*, vol. 172, p. 107670, July 2023.
- [43] T. Takaki, A. Yamanaka, Y. Higa, and Y. Tomita, “Phase-field model during static recrystallization based on crystal-plasticity theory,” *Journal of Computer-Aided Materials Design*, vol. 14, pp. 75–84, Dec. 2007.
- [44] L. Sharma, R. H. J. Peerlings, P. Shanthraj, F. Roters, and M. G. D. Geers, “An FFT-based spectral solver for interface decohesion modelling using a gradient damage approach,” *Computational Mechanics*, vol. 65, pp. 925–939, Apr. 2020.
- [45] Y. Chen, D. Vasiukov, L. Gélébart, and C. H. Park, “A FFT solver for variational phase-field modeling of brittle fracture,” *Computer Methods in Applied Mechanics and Engineering*, vol. 349, pp. 167–190, June 2019.
- [46] I. Jödicke, R. J. Leute, T. Junge, and L. Pastewka, “Efficient topology optimization using compatibility projection in micromechanical homogenization,” June 2022. arXiv:2107.04123 [cs].